

1 *Supplement of*

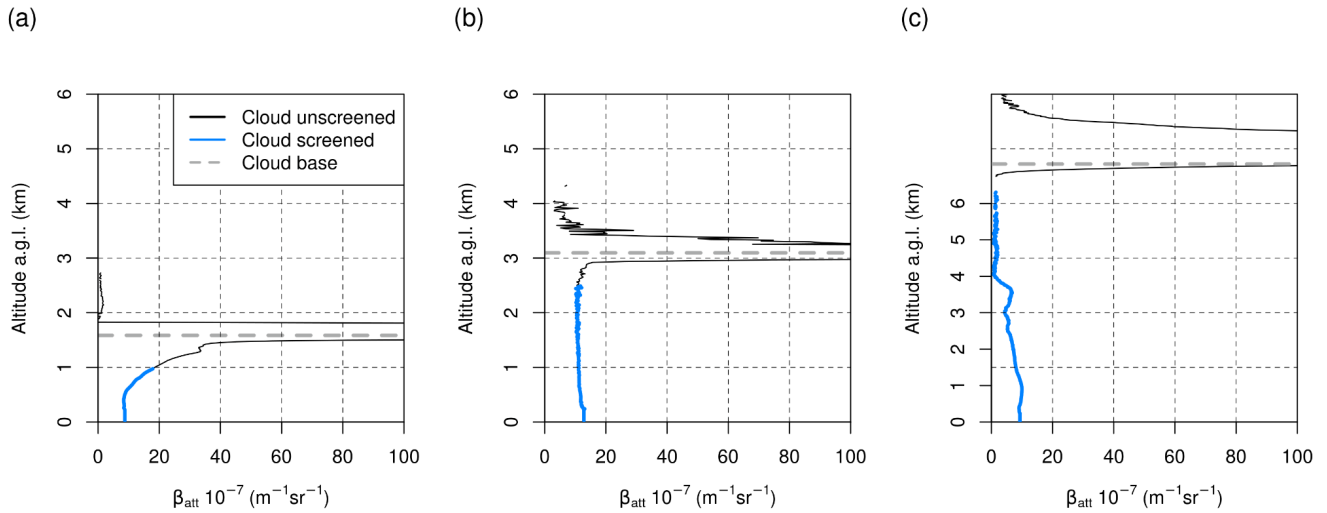
2 **ALICENET - An Italian network of Automated Lidar-Ceilometers**  
3 **for 4D aerosol monitoring: infrastructure, data processing, and**  
4 **applications**

5 **S1 Cloud screening**

6 To avoid contamination of aerosol retrievals by clouds and droplets the ALC signal is filtered out from 500 m below the  
7 Cloud Base Height (CBH) and above. The CBH provided by the ALC firmware is used for this purpose. The 500 m-buffer  
8 was conservatively chosen to limit the impact of variability in the CBH identification due to differences in instrument type  
9 and firmware version. A temporal cloud-filter is also applied, which removes signals collected 15 min before-to-15 min after  
10 the firmware cloud detection, using the same criteria as above and exploiting the nearest CBH measurements.

11 As an example of the effectiveness of the cloud screening procedure, Fig. S1 shows three different cloud-affected, 1-hour  
12 averaged total attenuated backscatter profiles before (black line) and after (blue line) the cloud-screening. The ALC  
13 measurements were collected in Aosta in the presence of low (Fig. S1a), medium (Fig. S1b), and high (Fig. S1c) clouds.

14



16

17 **Figure S1:** Examples of the ALICENET cloud screening on the total attenuated backscatter ( $\beta_{\text{att}}$ ) profiles derived from the CHM15k  
 18 signals in Aosta: (a) 19/06/2022 4-5 UTC, (b) 27/06/2022 11-12 UTC, (c) 18/06/2022 20-21 UTC. The x-axis was cut at  $100 \text{ m}^{-1} \text{ sr}^{-1}$  to  
 19 better highlight the aerosol profile. The cloud base heights identified by the ALC firmware are also reported (dashed line). Both  $\beta_{\text{att}}$   
 20 profiles and cloud base heights are 1-hour averaged.

## 21 S2 Overlap correction

22 The derivation of the overlap correction to be applied to the ALICENET CHM15k systems is based on the procedure of  
 23 Hervo et al. (2016), plus additional quality controls (QC.OVL, see also Table S1). The Hervo procedure first selects time  
 24 windows in which a nearly homogeneous aerosol layer in the first 1200 m can be assumed. Then, based on this homogeneity  
 25 assumption, for each selected time window it derives an overlap correction factor,  $f_c(r)$ , to be applied to the overlap  
 26 correction function provided by the manufacturer,  $\text{Ovl}_{\text{man}}(r)$ , so that the new overlap correction function is:

$$27 \text{Ovl}(r) = \frac{\text{Ovl}_{\text{man}}(r)}{f_c(r)} \quad (\text{S2.1})$$

28 The relative difference (RD) between the Ovl-corrected and the  $\text{Ovl}_{\text{man}}$ -corrected ALC signals is thus  $\text{RD}(r) = f_c(r) - 1$ .

29 As found by Hervo et al. (2016),  $f_c(r)$  is actually dependent on the system internal temperature, which exhibits a seasonal  
 30 cycle. To account for this dependence, an ensemble of  $f_c(r)$  is derived using an ALC dataset spanning different seasons, and

3  
4

31 each  $f_c(r)$  is related through a linear fit with the internal temperature of the system ( $T_{instr}$ ) within the corresponding time  
 32 window. This procedure gives a system-, range- and temperature-dependent ‘overlap model’  $Ovl_{model}(r,T)$ .  
 33 Since the assumption of aerosol homogeneity in the lowermost levels is particularly critical at some ALICENET stations, we  
 34 introduced specific quality controls to derive a robust  $Ovl_{model}(r,T)$ :

35 a) prior to the derivation of the overlap model, a filter (QC.OVL1) is applied on the ensemble of overlap correction  
 36 factors, in order to reject those likely derived in inhomogeneous conditions and thus leading to unrealistic overlap  
 37 corrections. Operationally, for each  $f_c(r)$  the following metric is calculated:

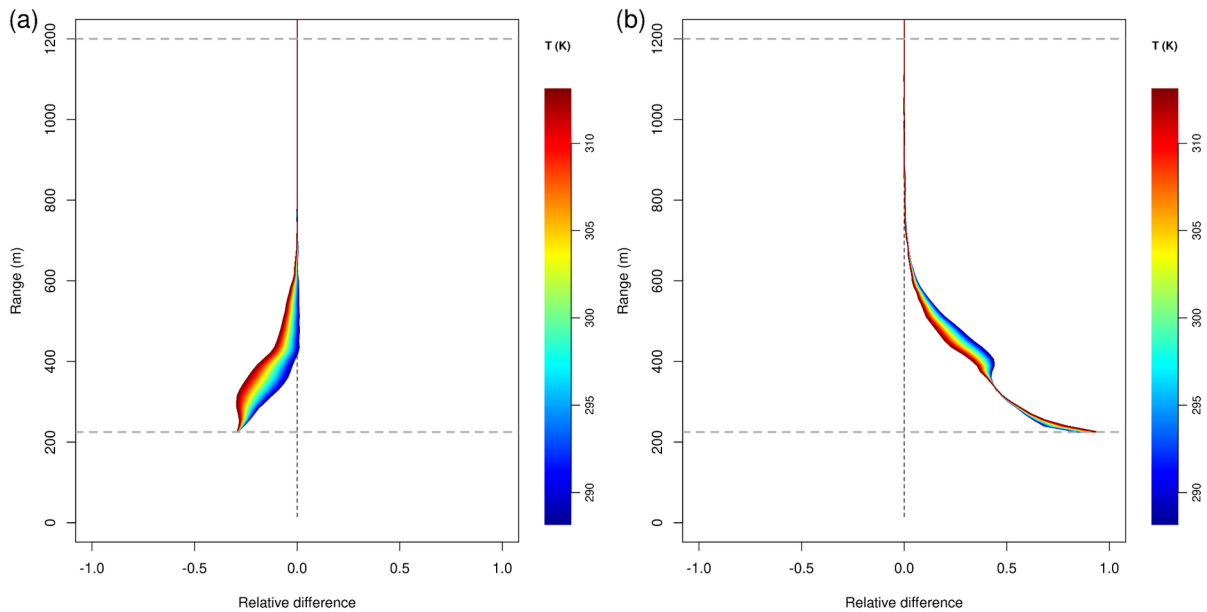
$$38 \quad M_{ov} = \sum \left( \frac{\text{median} \left( \left| RD(r) - RD_i(r) \right| \right)}{\left| T_{instr} - T_i \right|} \right) / N \quad (S2.2)$$

39 where  $RD$  and  $T_{instr}$  are the relative difference and the system internal temperature associated with the considered  
 40  $f_c(r)$ , the median is calculated over the vertical range 225-1200 m, and the sum is performed over the sub-ensemble  
 41 of system internal temperatures  $T_i$  and associated relative differences  $RD_i$  lying between  $\pm 5$  K from the considered  
 42  $T_{instr}$ . Then,  $f_c(r)$  associated with  $M_{ov} < 0.05$  are rejected;

43 b) the number of non-rejected overlap correction factors must be  $> 20$  (QC.OVL2);  
 44 c) an ALC dataset longer than one year must be used to obtain a statistically significant ensemble of overlap functions  
 45 spanning a representative range of temperature (QC.OVL3);

46 If the above QCs are met, the overlap model is derived using a robust linear fit (rlm R package).

47 Examples of the relative differences between the ALC signals as corrected with the ALICENET QC overlap models and the  
 48 manufacturer overlap functions are shown in Fig. S2, these referring to the Rome and Aosta CHM15k systems.



50 **Figure S2:** Range- (y axis) and temperature- (colour) dependent relative differences between the ALC signals corrected using the quality  
 51 controlled overlap models derived by ALICENET and the manufacturer overlap functions. The two plots refer to the overlap corrections  
 52 applied to the CHM15k systems in (a) Rome, and (b) Aosta.

53

54 Below 225 m a.g.l., the raw profiles are extrapolated down to the ground by linear fitting in winter (using data from 225 m to  
 55 285 m) or assuming a homogeneous profile below 225 m in summer, to avoid altitude ranges where the partial overlap is still  
 56 insufficient to derive quantitative information.

### 57 **S3 Absolute calibration**

58 The Rayleigh calibration procedure implemented in ALICENET is based on the comparison of the pre-processed ALC signal  
 59 with a theoretical molecular profile in aerosol free regions. The theoretical molecular backscatter profile at the operating  
 60 wavelength is derived using the Bodhaine formulation (Bodhaine, 1999) and site- and monthly-dependent temperature and  
 61 pressure profiles extracted from ERA5 reanalyses. The procedure is made of two steps: a) selection of the optimal molecular  
 62 window for calibration, and b) computation of the calibration coefficient  $C_L$ . Each step includes specific quality controls  
 63 (QC.CAL, see also Table S1).

64

65 a) The selection of the molecular window is performed considering nighttime-only profiles to avoid sunlight noise, and using  
 66 vertical profiles collected over 3-6 hours, depending on cloudiness, and between 3-7 km a.g.l. Along this vertical range, an  
 67 iterative procedure is applied over an ensemble of ‘potential’ molecular windows centred at different altitudes and with  
 68 variable amplitudes, these ranging from 600 to 3000 m at steps of 30 m. For each potential range-window, i.e., combination  
 69 of central altitude and amplitude, the linear fit between the time-window-averaged signal and the theoretical molecular  
 70 attenuated backscatter profile is performed. In order to reject those range-windows still affected by aerosol loads, a test is  
 71 performed to check for the presence of coherent structures therein. More specifically, the Breusch-Godfrey test (BG test;  
 72 Breusch, 1978) is applied to calculate the autocorrelation in fit residuals. The windows associated with p-value of the BG  
 73 test  $> 0.05$  are rejected (QC.CAL1). From the ensemble of retained windows, the molecular window selected for the  
 74 calibration is the one maximising a metric ( $M_{ray}$ ) defined as follows:

$$75 \quad M_{ray} = \frac{adjR^2 + (1 - |b|)}{std(b)} \quad (S3.1)$$

76 where  $adjR^2$  and  $b$  represent the adjusted  $R^2$  and the intercept of the linear fit, respectively, and  $std(b)$  the standard deviation  
 77 of  $b$  over the ensemble of potential molecular windows. In particular, the adjusted  $R^2$  is calculated as:

$$78 \quad adjR^2 = 1 - \frac{(1 - R^2)(n - 1)}{(n - k - 1)} \quad (S3.2)$$

79 where  $n$  is the number of data points within the molecular window and  $k$  the number of predictor variables.  
 80 The following quality controls are then further performed:

- 81 - the slope of the linear fit must be positive and the intercept nearly 0 (QC.CAL.2);
- 82 - the autocorrelation (BG test) and the cumulative sign in fit residuals at the window borders ( $\pm 200$  m from each  
 83 border) must be  $> 0.05$  and  $< 0$ , respectively (QC.CAL.3). This quality control is effective to filter the range  
 84 windows that sit over an undetected aerosol layer but are associated with a misleading robust linear regression with  
 85 the molecular profile.

86 If one of these QCs is not met, the night is rejected for calibration purposes, and the process continues using data from the  
 87 following night.

88

89 b)  $C_L$  computation. Once the molecular window is selected, the backward Klett inversion (Klett, 1985) is applied for the  
 90 inversion of the time-window-averaged ALC signal into the total attenuated  $\beta_{att}$  profile. Note that the sign correction in the  
 91 Klett algorithm reported by Speidel and Vogelmann (2023) was already introduced in the ALICENET procedure since the  
 92 beginning of its activities. The  $C_L$  is derived as (Wiegner and Geiß, 2014):

$$93 \quad C_L = \text{median} \left( \frac{P(r) \frac{r^2}{Ovl}(r)}{\beta_{at}(r)} \right) \quad (S3.3)$$

94 where  $P(r) r^2 / Ovl$  is the time-window-averaged range- and overlap-corrected ALC signal, and the median is calculated  
 95 along the identified molecular range-window.

96 Two further quality controls are then performed at this stage:

- 97 - calibration coefficients associated with relative uncertainty  $E_{CL} > 40\%$  are rejected (QC.CAL.4). The calibration  
 98 coefficient relative uncertainty is defined as follows:

$$99 \quad E_{CL} = \frac{\text{err}(C_L^{\text{slope}})}{C_L^{\text{slope}}} + \frac{\text{std}(C_L)}{\text{median}(C_L)} \quad (S3.4)$$

100 In the first term,  $C_L^{\text{slope}}$  represents the slope of the fit between the ALC signal and the theoretical molecular  
 101 backscatter profile within the molecular range-window, and  $\text{err}(C_L^{\text{slope}})$  the standard error of the slope. In the second  
 102 term,  $\text{median}(C_L)$  and  $\text{std}(C_L)$  represent the median and the standard deviation of the calibration coefficient as  
 103 derived in Wiegner and Geiß (2014) within the molecular range-window, respectively;

- 104 - calibration coefficients leading to a negative AOD are rejected (QC.CAL.5). This quality control is effective in  
 105 filtering those  $C_L$  associated with calibration windows containing residual aerosols. In such cases, the aerosol  
 106 extinction coefficient resulting from the Klett inversion can assume slightly negative values and lead to a negative  
 107 sign of the AOD.

108 Determination of  $C_L$  can be hampered in periods of unfavourable atmospheric conditions or high aerosol loads in the middle  
 109 troposphere, where the calibration window is generally selected. Moreover, the  $C_L$  coefficients of different ALICENET  
 110 systems were observed to follow a seasonal cycle (see Fig. 5 and related text) as also observed in other European ALC  
 111 networks. At present, the  $C_L$  values operationally applied in ALICENET inversions are interpolated in time using a non-  
 112 parametric regression of the  $C_L$  coefficients. More specifically, a locally weighted smoothing (Loess) fit with a time span  $> 1$   
 113 year (tunable) is used.

## 114 **S4 Retrieval of aerosol properties**

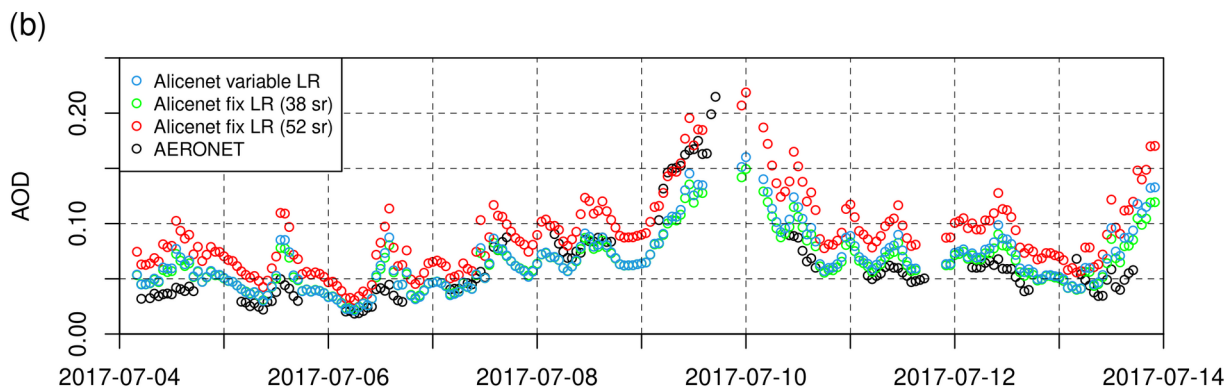
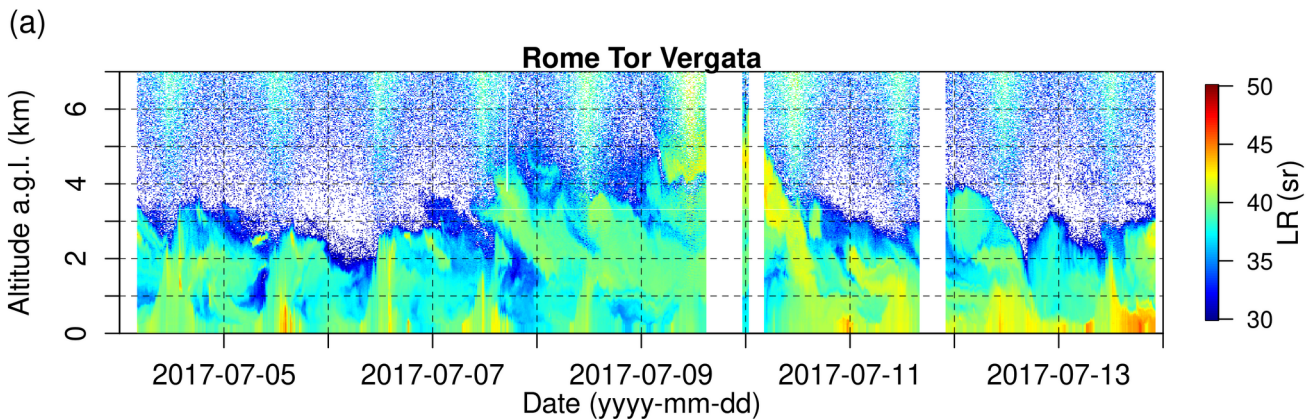
### 115 **S4.1 Aerosol optical properties**

116 In ALICENET, the aerosol backscatter ( $\beta_p$ ) and extinction ( $\alpha_p$ ) are retrieved from Eq. 1 using the forward Klett inversion. To  
 117 this purpose these two unknowns of Eq. 1 are linked one to the other through the functional relationship  $\alpha_p = \alpha_p(\beta_p)$  derived  
 118 using a continental aerosol model by Dionisi et al. (2018). Operatively, an iterative procedure is applied within the forward  
 119 Klett inversion to derive  $\beta_p(r)$  and  $\alpha_p(r)$  vertical profiles as follows:

- 120 1. the procedure starts from a first-guess, vertically-constant Lidar Ratio (LR) profile of 38 sr, this being similar to the
- 121 value used in the NASA-CALIPSO inversion at 1064 nm for clean/polluted continental aerosol (Omar et al., 2009);
- 122 2. the LR profile is then updated at each iteration based on the  $\alpha_p = \alpha_p(\beta_p)$  functional relationship;
- 123 3. the iterations stop when convergence on the final  $\beta_p$  profile is reached. More specifically, the established
- 124 requirement is that the difference of the vertically integrated aerosol backscatter in two successive iterations keeps <
- 125 0.0025 m<sup>-1</sup> sr<sup>-1</sup>.

126 The iterative procedure has the ability to ‘adjust’ the first-guess, vertically-constant LR profile according to the actual  
127 aerosol stratification. An example of the ‘adjusted’, vertically-variable LR profiles is shown in Fig. S3a, this referring to the  
128 same period addressed in Fig. 6. It is worth mentioning that a main advantage of the variable-LR method is the fact that it is  
129 independent from ancillary (e.g., sunphotometer) data and a-priori assumptions (e.g., the actual LR value to be used), thus  
130 allowing an automatic, ALC-based, homogeneous retrieval of aerosol properties in different sites and periods. As reported in  
131 the main text (Fig. 7) and further shown in Dionisi et al. (2018), the ALICENET-retrieved aerosol optical properties were  
132 found in good agreement with independent sunphotometer data in different sites. A comparison of the performances of the  
133 adjusted-LR and fixed-LR approaches was also conducted by Dionisi et al. (2018) using ALC data from different stations. In  
134 brief, the authors found a good agreement between sunphotometer and ALC-based AOD using both the iterative procedure  
135 and a fixed LR of 38 sr, and larger discrepancies using a fixed LR of 52 sr, regardless of the site location. As an example, in  
136 Fig. S3b we show a short-term comparison of the AOD retrieved with both ALICENET processing and fixed-LR values  
137 (chosen as in Dionisi et al., 2018) and the reference AERONET L2 AOD in the same period presented in Fig. 6.

138



140

141 **Figure S3:** (a) Variable Lidar Ratio (LR) profiles derived within the ALICENET processing on the CHM15k operating in Rome - Tor  
 142 Vergata in the same period presented in Fig. 6; (b) AOD retrieved with both ALICENET processing and fixed-LR values (chosen as in  
 143 Dionisi et al., 2018) compared to reference AERONET L2 data.

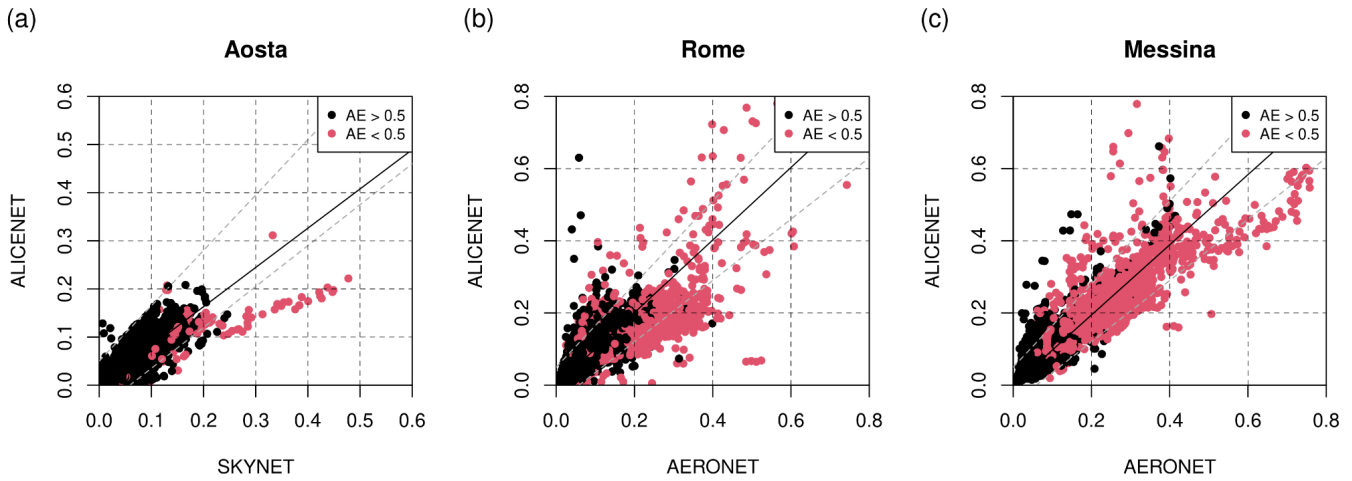
144

145 In the main text we evaluated the overall performances of the ALICENET retrieval of aerosol optical properties using multi-  
 146 annual datasets of three ALICENET systems located in very different environments (Fig. 7). Here, we further explore the  
 147 reasons for main discrepancies. In particular, Fig. S4 shows the same data of Fig. 7, with separation of data pairs based on  
 148 the photometer-derived Ångström Exponent. It shows that most deviations from the 1:1 line are associated to coarse-mode  
 149 dominated aerosol types ( $AE < 0.5$ , red), likely due to desert dust or sea-salt particles, thus deviating from the continental  
 150 aerosol model assumed for the derivation of the functional relationships used in the ALC data inversion.

151

15  
 16





152 **Figure S4:** Same as Figure 7, but separating data pairs associated with a sunphotometer-derived Ångström Exponent (AE) < 0.5 (red) and  
 153 > 0.5 (black).

#### 154 S4.2 Aerosol physical properties

155 In the main text (Sect. 3.3.2) we discussed the need to estimate ‘dry’ aerosol mass concentrations from ALC-based ‘wet’  
 156 aerosol profiles when aiming at the direct comparison with reference in-situ instrumentation. In such cases, we derive the dry  
 157 aerosol mass concentrations,  $M_p^{\text{dry}}$ , from the ALC (wet) aerosol mass concentrations,  $M_p$ , following Adam et al. (2012):

$$158 \quad M_p^{\text{dry}} = \frac{M_p^{\text{dry}}}{1 + \frac{1}{\rho_d} (GF^3 - 1)} \quad (\text{S4.1})$$

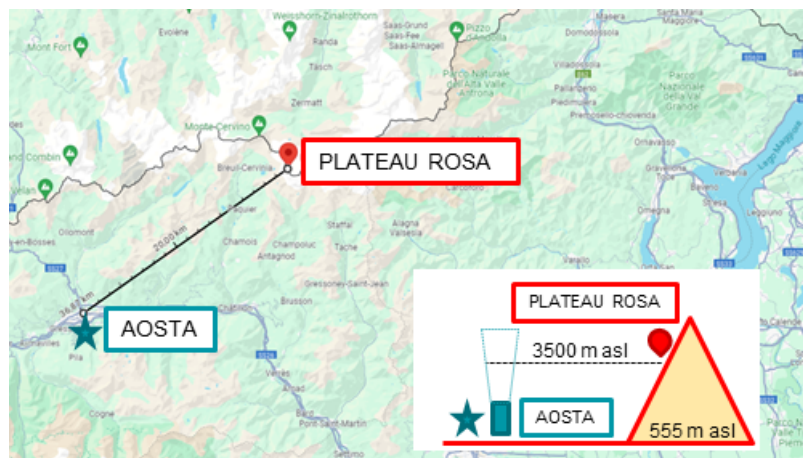
159 where

$$160 \quad GF = \left( 1 - \frac{RH}{100} \right)^{-\gamma} \quad (\text{S4.2})$$

161 is the hygroscopic growth factor and RH the ambient relative humidity. The values of the dry aerosol density  $\rho_d$  and of the  $\gamma$   
 162 exponent depend on the aerosol mixture under investigation and are the main sources of uncertainty in the aerosol mass  
 163 retrieval (Adam et al., 2012; see also main text, Sect. 3.3.3). Their accuracy strongly depends on the possibility to identify  
 164 the actual, dominant aerosol type, e.g., through depolarisation information and/or model data.

165 An example of this RH-correction was reported in Fig. 8 (see main text), which shows the comparison between the  
 166 ALICENET-derived  $M_p^{\text{dry}}$  and the in-situ  $PM_{10}$  measurements from an OPC operating at the high altitude (3500 m a.s.l.)  
 167 station Testa Grigia - Plateau Rosa (data courtesy of Stefania Gilaroni CNR-ISP) in June 2022. The ALICENET aerosol

168 mass concentrations were retrieved from the CHM15k operating in Aosta, which is about 35 km apart from Testa Grigia (see  
169 Fig. S5), considering data in the vertical range  $3500 \pm 200$  m a.s.l.

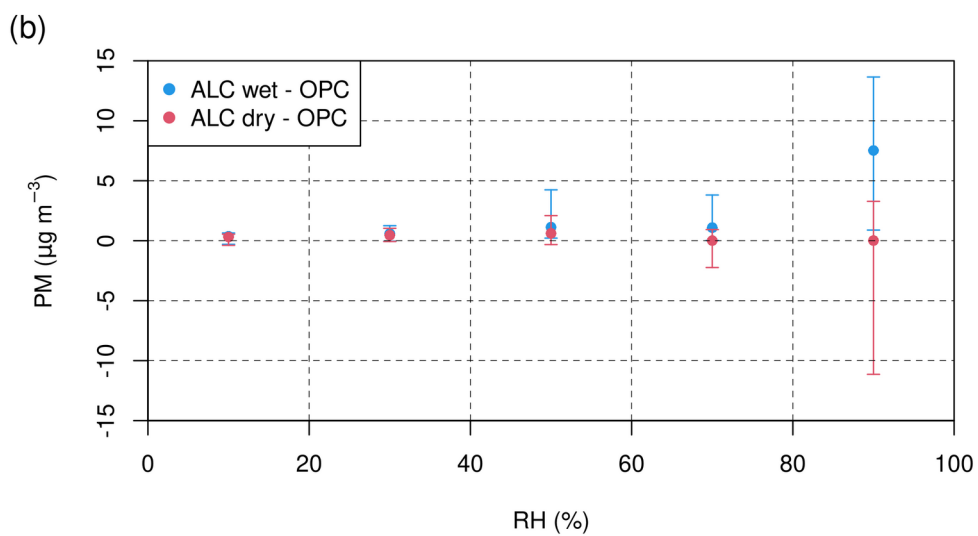
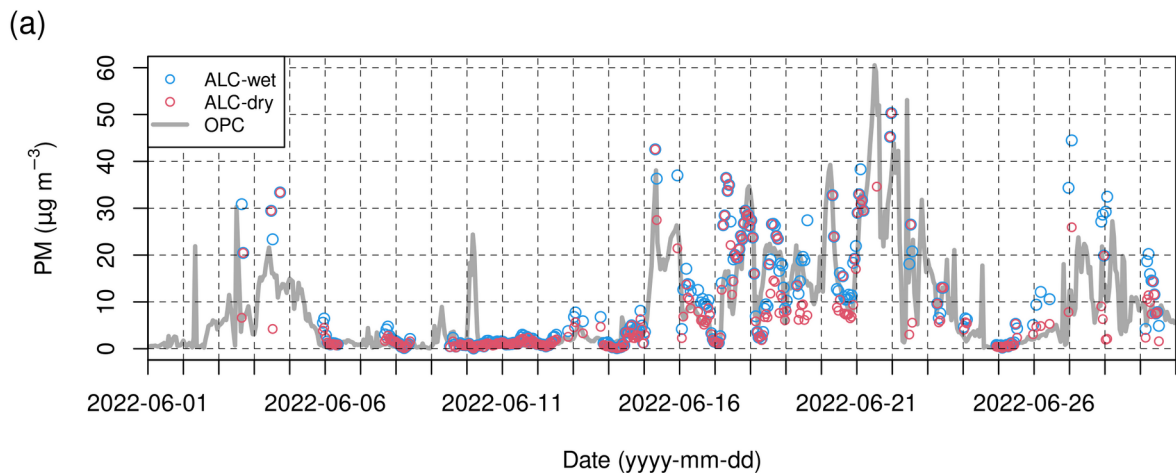


171 **Figure S5:** Map with the locations of the Aosta and Testa Grigia - Plateau Rosa stations (35 km apart). In the bottom-right corner, a  
172 scheme with the station altitudes is also reported. Background Map credits: © Google Maps.

173

174 In that case,  $\gamma = 0.2$  in the presence of continental, hygroscopic aerosols (D'Angelo et al., 2016) and  $\gamma = 0$  (i.e.,  $M_p^{\text{dry}} = M_p$ )  
175 in the presence of dust, hydrophobic particles (Barnaba et al., 2010). The aerosol type was assessed through the linear  
176 volume depolarisation ratios ( $\delta_v$ ) profiles of a co-located PLC, assuming that aerosol mixtures associated with  $\delta_v < (>) 15\%$   
177 are dominated by continental (dust) particles. The RH was extracted from the dataset of the high-resolution atmospheric  
178 model MERIDA (Bonanno et al., 2019). During the period addressed in Fig. 8, at the altitude of Testa Grigia - Plateau Rosa  
179 the simulated RH ranged from 16% to 98%, and the measured  $\delta_v$  from 0.4% to 27%. In Fig. S6a we further show the same  
180 data including both RH-non corrected (wet, blue bullets) and RH-corrected (dry, red bullets) aerosol mass concentrations as  
181 retrieved by ALICENET. The median difference between the ALC-based wet/dry aerosol mass concentrations and the OPC  
182  $PM_{10}$  measurements was evaluated as a function of RH in Fig. S6b. It shows the median differences between ALC- and  
183 OPC-based aerosol mass concentrations per RH bins, with dry values keeping around zero. On average, the hygroscopic  
184 correction reduced the difference between ALC and OPC mass estimates, but the large horizontal distance between Aosta  
185 and Testa Grigia - Plateau Rosa and the uncertainty of the ALICENET aerosol volume retrieval in dust conditions strongly  
186 complicate the evaluation of this correction.

187



189

190 **Figure S6:** (a) Same as Figure 8, but including both wet (blue bullets) and dry (red bullets) aerosol mass concentrations as retrieved by  
 191 ALICENET; (b) Median differences (points) and 25-75 percentiles between ALC- and OPC-based aerosol mass concentrations per  
 192 RH bins (0-20%, 20-40%, 40-60%, 60-80%, 80-100%) for data reported in panel (a).

193

195 The monitoring capability of ALCs offers the opportunity to have continuous, accurate information of the aerosol vertical  
 196 distribution. While several tools are already available for the ALC-based detection of the atmospheric boundary layer and  
 197 mixed layer heights (e.g., Kotthaus et al., 2020, 2023), a specific need in the Italian context was also the further automatic  
 198 identification of lofted aerosol layers. We thus developed an original tool (ALADIN: Aerosol LAYer DetectIoN) to identify  
 199 main aerosol stratifications from ALC/PLC L2 profiles. The aerosol layers targeted by ALADIN are: 1. the Continuous  
 200 Aerosol Layer (CAL), i.e., the layer continuously dominated by aerosols from the ground level up to its upper boundary; 2.  
 201 the Mixed Aerosol Layer (MAL), this being a CAL sublayer within which particles are mixed by turbulent fluxes; 3.  
 202 Elevated Aerosol Layers (EALs), i.e., lofted aerosol layers that are located above the MAL and either within or above the  
 203 CAL. The ALADIN procedures for the detection of CAL, MAL, and EALs are described hereafter and summarised in Fig.  
 204 S8.

- 205
- 206 1. The CAL height (CALH) is derived from cloud-screened, denoised  $\beta_{\text{att}}$  profiles averaged at 30 min resolution. It is  
 207 simply defined as the altitude of the layer extending from the surface and in which  $\beta_{\text{att}} > \beta_{\text{mol}}$  for at least 98% of its  
 208 extension. The CALH search is performed in the vertical range 225-7000 m a.g.l.
  - 209 2. The MAL is identified through a technique highlighting regions where aerosols are mixed by vertical turbulent  
 210 fluxes. The procedure is made of two steps: a) the estimation of vertical aerosol fluxes and b) an associated variance  
 211 analysis.  
 212 a) We estimate vertical aerosol fluxes by applying a Dynamic Time Warping algorithm (DTW, Giorgino et al.,  
 213 2009) to a sequence of  $\beta_{\text{att}}$  profiles at relatively high (1-min) resolution. In brief, this algorithm computes the local  
 214 stretch or compression to be applied to the  $\beta_{\text{att}}$  sequence in order to optimally link each profile to the following one.  
 215 An example of the output field of the DWT procedure,  $w_{\text{DTW}}$ , is given in Figure S7a for the same episode addressed  
 216 in Fig. 6. The variable  $w_{\text{DTW}}$  can be interpreted as the local vertical displacement of the aerosol-loaded air parcels  
 217 (i.e., similar to a vertical velocity), thus the region near the surface where it rapidly changes in sign and magnitude  
 218 highlights where the mixing is acting.  
 219 b) The variance analysis of  $w_{\text{DTW}}$  allows us to identify the MAL height (MALH). First, we compute the standard  
 220 deviation of  $w_{\text{DTW}}$  ( $\sigma_w$ ) over 30 min intervals as generally done in Eddy-Covariance analysis (Aubinet et al., 1999).  
 221 The MAL height at time  $t$ ,  $\text{MALH}(t)$ , is then defined as the height of the first  $\sigma_w$  local minima which:  
 222 - lies within  $\text{MALH}(t-\Delta t) - 600$  m and  $\text{MALH}(t-\Delta t) + 1200$  m during the morning, and  $\text{MALH}(t-\Delta t) + 600$   
 223 m and  $\text{MALH}(t-\Delta t) - 1200$  m during the afternoon, with  $\Delta t=30$  min;  
 224 - minimises the following metric:  
 225

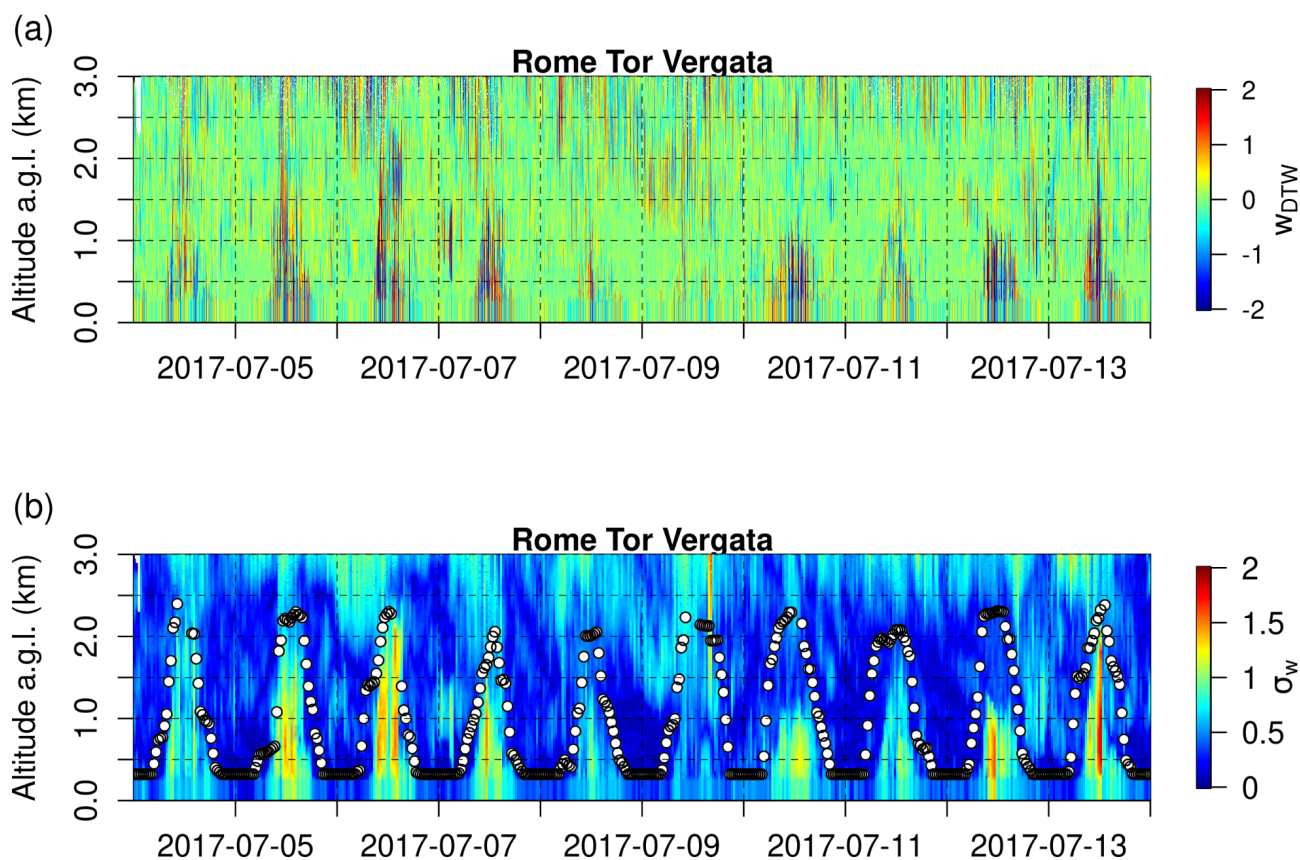
226 
$$M_{mal} = |z_{min} - MALH(t - \Delta t)| + \frac{1}{median(\sigma_w)} \quad (S5.1)$$

227 where  $z_{min}$  denotes the height of the  $\sigma_w$  local minima, and the median is calculated along the vertical range  
228 225 m -  $z_{min}$ .

229 The  $\sigma_w$  field together with the identified MAL heights are shown in Fig. S7b (same period as Fig. 6).

230 The search of MALH is performed:

- 231 - below CALH and within site- and season-dependent maximum and minimum values defined by the user.  
232 For example, in Rome-Tor Vergata a maximum height of 3500 (2500) m is set during summer (winter). In  
233 general, the MAL lower limit must be higher than the height of the ALC blind overlap region, which is  
234 approximately 225 m for CHM15k systems and few tens of metres for CL61 systems;  
235 - from 1 hour before sunrise to 1 hour after sunset, where the site- and season-dependent sunrise/sunset  
236 hours are calculated using the Michalsky algorithm (Michalsky, 1988).



238 **Figure S7:** (a) Output field of the Dynamic Time Warping algorithm ( $w_{DTW}$ ) applied to the  $\beta_{att}$  profiles of the CHM15k operating in  
 239 Rome-Tor Vergata in the same period presented in Fig. 6, and (b) 30-min standard deviation of  $w_{DTW}$  ( $\sigma_w$ ) and corresponding Mixed  
 240 Aerosol Layer (MAL) heights (white points) identified by the ALADIN procedure.

241

242 3. The EALs are detected from cloud-screened and denoised  $\beta_{att}$  profiles averaged at 30 min resolution. The  
 243 procedure, which includes specific quality controls (QC.EAL, see also Table S1), is made of two steps: a) the  
 244 detection of the presence of elevated layers, and b) the identification of their top and bottom boundaries.

245 a) We identify lofted aerosol layers using the Continuous Wavelet Transform (CWT) algorithm developed by Du et  
 246 al. (2006). This algorithm, referred to as CWT+, has the advantage of discriminating signal peaks attributable to  
 247 aerosol layers from noise spikes by analysing both  $\beta_{att}$  and CWT coefficients. The peak detection is performed from  
 248 MALH up to 7 km a.g.l.

27  
 28

249 b) For each detected aerosol layer, we derive the top and bottom boundaries ( $EAL_{top}$  and  $EAL_{bottom}$ , respectively)  
 250 with an iterative technique. Operatively, an ensemble of potential bottom and top boundaries is considered, and for  
 251 each bottom-top combination the following metric is calculated:

$$252 \quad M_{eal} = \frac{\int \beta_{att}(r) dr}{\int \beta_{ref}(r) dr} + Perc(\beta_{att} > \beta_{ref}) + G_{border} + CWT_{border} \quad (S5.2)$$

253 where  $\beta_{ref}$  denotes a ‘reference’ total attenuated backscatter profile, the integrals are calculated along the bottom-top  
 254 range, Perc represents the percentage of points with  $\beta_{att} > \beta_{ref}$  along the bottom-top range,  $G_{border}$  denotes the  
 255 normalised mean gradients of  $\beta_{att}$  and  $CWT_{border}$  the normalised mean CWT coefficients along the vertical ranges  
 256  $EAL_{top} \pm 90$  m and  $EAL_{bottom} \pm 90$  m.

257 The EAL vertical range is selected as the top-bottom combination maximising the  $M_{eal}$  metric.

258 It is worth highlighting that, with this approach, the choice of  $\beta_{ref}$  depends on the application. Molecular attenuated  
 259 backscatter profiles are used as reference when the aim is to detect aerosol layers with respect to a clean  
 260 atmosphere, while ‘climatological’ site-dependent  $\beta_{att}$  profiles, such as the ones derived from our multi-annual  
 261 datasets, are used to identify anomalous aerosol layers with respect to the typical aerosol conditions (Bellini et al.,  
 262 2024, in preparation).

263 Finally, three conditions must be fulfilled to identify an EAL:

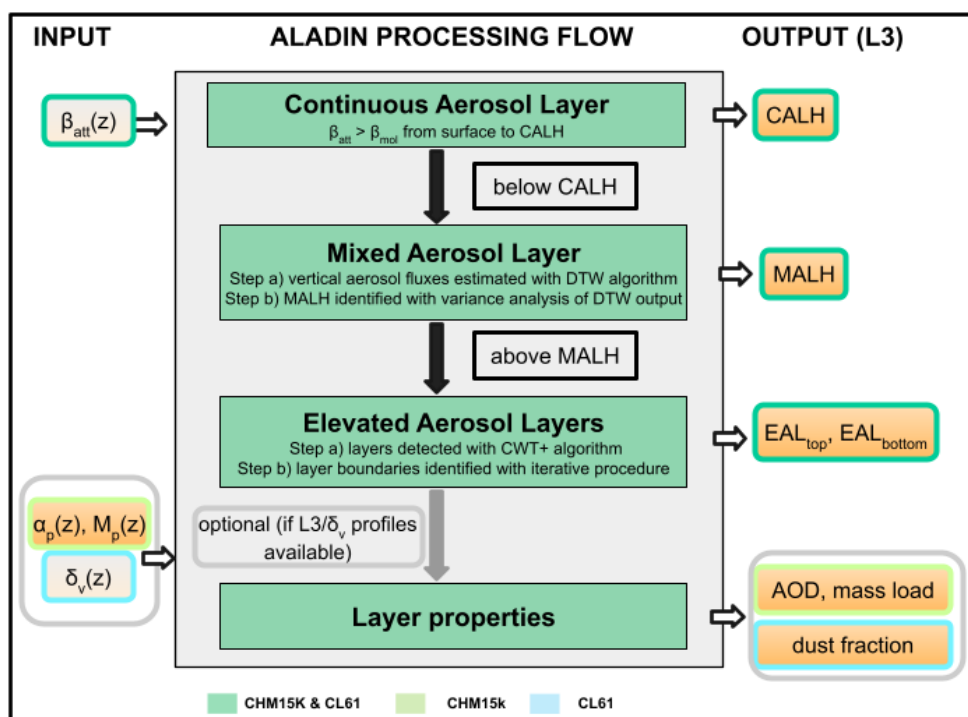
- 264 - within the layer it should be  $Perc(\beta_{att} > \beta_{ref}) > 90\%$  (QC.EAL.1) and  $\int \beta_{att}(r) dr > \int \beta_{ref}(r) dr$  (QC.EAL.2);
- 265 - it should be  $G_{border} < 0$  at the EAL top,  $G_{border} > 0$  at the EAL bottom, and  $CWT_{border} < 0$  at both boundaries  
 266 (QC.EAL.3).

267  
 268 When corresponding L3 inversions or PLC linear volume depolarisation ratio ( $\delta_v$ ) profiles are available, mean  
 269 properties of the aerosol layers can also be derived, such as the layer AOD and mass load, or the mean fraction of  
 270 irregular (generally dust) particles within the layer,  $F_d$ . In the last case, we exploit the PLC  $\delta_v$  profiles as follows  
 271 (Tesche et al., 2009):

$$272 \quad F_d = median \left( \frac{(\delta_v - \delta_{nd})(1 + \delta_d)}{(\delta_d - \delta_{nd})(1 + \delta_v)} \right) \quad (S5.3)$$

273 where  $\delta_d$  and  $\delta_{nd}$  are the typical linear volume depolarisation ratios of dust and non-dust particles, respectively, and  
 274 the median is calculated along the layer bottom-top range. The values of  $\delta_d$  and  $\delta_{nd}$  are generally set to 25% and 5%,  
 275 respectively (e.g., Haarig et al., 2022).

276



278

279 **Figure S8:** Scheme of the ALADIN processing flow from the input total attenuated backscatter ( $\beta_{\text{att}}$ ) profiles to L3 output products. As in  
 280 Fig. 2, the different box contour colours are used to indicate products valid for CHM15k ALCs (light green), CL61 PLCs (cyan), or both  
 281 (dark green) systems. Relevant L3 output products include the Continuous Aerosol Layer Height (CALH), the Mixed Aerosol Layer  
 282 Height (MALH), and the top and bottom boundaries of Elevated Aerosol Layers ( $\text{EAL}_{\text{top}}$  and  $\text{EAL}_{\text{bottom}}$ , respectively). Optionally, if L3  
 283 profiles of aerosol properties (such as aerosol extinction,  $\alpha_p$ , and mass concentrations,  $M_p$ ) or volume linear depolarisation ratio ( $\delta_v$ )  
 284 profiles are available, specific properties of the aerosol layers can be derived, such as the layer Aerosol Optical Depth (AOD), mass load,  
 285 or dust fraction.

286

## 287 **S6 Summary of quality controls within the overall ALICENET processing chain**

288 In Table S1, we summarise the quality controls (QCs) discussed above and associated with the overlap correction  
 289 (QC.OVL), the absolute calibration (QC.CAL), and the ALADIN detection of elevated aerosol layers (QC.EAL).

290



ALICENET processing step (Supplement Section)	Quality Controls (QCs)
Overlap correction (S2)	QC.OVL1: it filters out of the ensemble unphysical overlap corrections QC.OVL2: it ensures that the overlap model is derived over a statistically significant dataset QC.OVL3: it ensures that the temperature-dependent overlap model is derived over an ensemble spanning a representative range of temperatures
Absolute calibration (S3)	QC.CAL1: it filters potential calibration (molecular) windows that are affected by the presence of aerosol layers within their boundaries QC.CAL2: it ensures that the parameters of the fit between the ALC signal and the theoretical molecular profile lie within physical ranges QC.CAL3: it ensures that the calibration window is not located over an homogeneous aerosol layer QC.CAL4: it filters calibration coefficients that are associated with unacceptable relative uncertainties QC.CAL5: it filters calibration coefficients that lead to a negative aerosol optical depth in the vertical range 0-4 km a.g.l.
ALADIN detection of elevated aerosol layers (S5)	QC.EAL1: it ensures that the percentage of points exceeding a reference profile within the EAL top-bottom range is greater than 90% QC.EAL2: it ensures that the integrated aerosol backscatter within the EAL top-bottom range is greater than the one obtained with the reference profile QC.EAL3: it ensures that the $\beta_{\text{att}}$ gradient and CWT coefficients at the layer borders are consistent with the presence of an aerosol layer

291

292 **Table S1:** Summary of Quality Control (QC) criteria applied within the different steps of the ALICENET processing chain.

293

294 Additional quality assurance (QA) criteria are applied on ALICENET aerosol products when investigating their temporal  
 295 and vertical variability, as performed within the long-term analysis of aerosol properties and layering in selected ALICENET  
 296 sites (Bellini et al., in preparation, 2024). It is worth mentioning that several requirements are also applied for the detection  
 297 of the CAL and MAL heights, such as maximum/minimum altitudes of the search regions and maximum/minimum vertical  
 298 increments between two successive time steps. However, these are not classified as QCs, as they are applied before the layer  
 299 detection to support the spatio-temporal continuity of the CAL and MAL retrievals.